

Formulation and characterisation of resveratrol-loaded nanostructured lipid carriers for use in combination with scalp cooling therapy to mitigate chemotherapy-induced follicular cytotoxicity and hair loss

TOTEA, AM http://orcid.org/0000-0003-0974-7648, THOMAS, A, GEORGOPOULOS, Nik http://orcid.org/0000-0002-6330-4947 and CONWAY, BR http://orcid.org/0000-0001-5570-3318

Available from Sheffield Hallam University Research Archive (SHURA) at:

https://shura.shu.ac.uk/36332/

This document is the Published Version [VoR]

Citation:

TOTEA, AM, THOMAS, A, GEORGOPOULOS, Nik and CONWAY, BR (2026). Formulation and characterisation of resveratrol-loaded nanostructured lipid carriers for use in combination with scalp cooling therapy to mitigate chemotherapy-induced follicular cytotoxicity and hair loss. Journal of Drug Delivery Science and Technology, 115 (1): 107671. [Article]

Copyright and re-use policy

See http://shura.shu.ac.uk/information.html

ELSEVIER

Contents lists available at ScienceDirect

Journal of Drug Delivery Science and Technology

journal homepage: www.elsevier.com/locate/jddst



Formulation and characterisation of resveratrol-loaded nanostructured lipid carriers for use in combination with scalp cooling therapy to mitigate chemotherapy-induced follicular cytotoxicity and hair loss

A.M. Totea a,c,* , A. Thomas , N.T. Georgopoulos b,1 , B.R. Conway c,d,1

- ^a School of Science, Faculty of Engineering and Science, University of Greenwich, Central Avenue, Chatham, ME4 4TB, UK
- ^b Biomolecular Sciences Research Centre, School of Biosciences and Chemistry, Sheffield Hallam University, Sheffield, S1 1WB, UK
- Department of Pharmacy, School of Applied Sciences, University of Huddersfield, Huddersfield, HD1 3DH, UK
- ^d Institute of Skin Integrity and Infection Prevention, University of Huddersfield, Huddersfield, HD1 3DH, UK

ARTICLE INFO

Keywords:
Chemotherapy
Alopecia
Nanostructured lipid carriers
Resveratrol
Scalp cooling
Antioxidants

ABSTRACT

Hair loss represents a highly traumatic side-effect of chemotherapy treatment, it significantly affects psychological well-being, self-esteem and quality-of-life, with the fear of alopecia causing severe anxiety for cancer patients. While effective in eliminating cancer cells, chemotherapy drugs collaterally damage hair follicles resulting in chemotherapy-induced alopecia (CIA). Scalp cooling is a breakthrough treatment for patients, being the only clinically proven method to prevent CIA, with 50–65 % of patients experiencing low grade alopecia (thus negating use of head covers and/or wigs during treatment).

Our recent biological studies showed that optimal cooling effectively protects cells in human hair follicles from chemotherapy drug-mediated damage, whereas suboptimal cooling is less effective. However, combining cooling with an antioxidant that blocks reactive oxygen species (ROS) restores this protective effect against chemotherapy-induced hair follicle damage.

In this study we focused on encapsulating the antioxidant resveratrol (RV) in nanostructured lipid carriers (NLCs) to optimise follicular targeting as a precursor to scalp cooling. We aimed for a particle size above 200 nm to limit systemic absorption and found that the nanoparticles had the desired properties when formulated with propylene glycol dicaprylate as the liquid lipid. RV-loaded NLCs remained stable at 4° C for >6 months, with less than 10 % variation in their size, polydispersity index (PDI), and zeta potential (ZP). Transmission electron microscopy (TEM) confirmed formation of Type I NLCs, featuring imperfect crystals that suggest a disordered lattice, facilitating RV's presence as disordered crystals or amorphous clusters within the matrix. Skin deposition studies demonstrated that RV-loaded NLCs reach the follicular reservoir within 6 h, confirming their potential for co-application with scalp cooing for combating CIA.

1. Introduction

Globally, 20 million people were diagnosed with cancer in 2022, and this number is projected to rise to over 35 million by 2050 [1,2]. The increasing incidence of cancer diagnoses has led to a rise in the number of patients requiring first-course chemotherapy that is critical for controlling and eliminating cancer cells but also associated with a heightened risk of alopecia. Chemotherapy medications, although effective in targeting cancer cells, often impact other cells with high proliferative activity, such as those found in hair follicles, including the rapidly

growing and proliferating matrix keratinocytes located in the hair bulb [3,4]. This can result in considerable hair loss or total alopecia, which can significantly affect a patient's emotional state and overall quality-of-life. Chemotherapy induced alopecia (CIA) is a highly devastating side effect for cancer patients that can affect up to 60 % of those undergoing treatment [5–7]. For many patients, hair loss is not merely a physical change; it also has a profound psychological and emotional impact, affecting their self-esteem and identity during an already challenging time. Its effects frequently result in intense anxiety, and this can even lead patients to decline treatment because of

^{*} Corresponding author. School of Science, Faculty of Engineering and Science, University of Greenwich, Central Avenue, Chatham, ME4 4TB, UK. *E-mail address:* a.totea@gre.ac.uk (A.M. Totea).

 $^{^{1}}$ Joint senior authors.

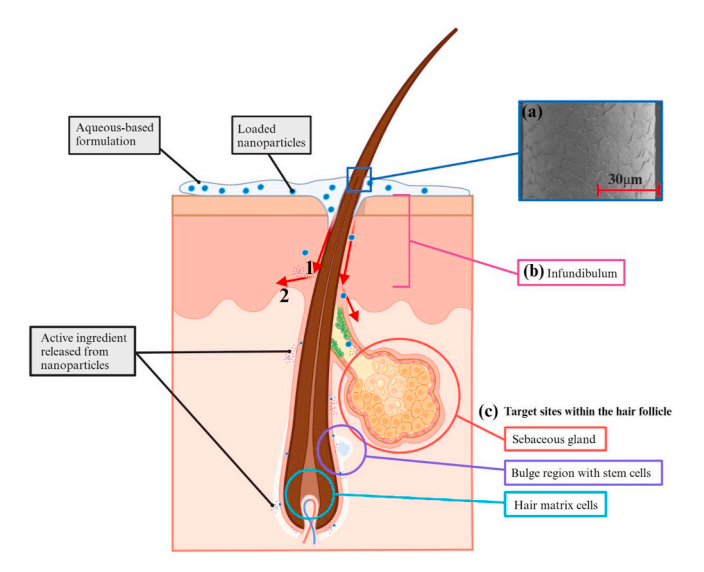


Fig. 1. Key processes involved in hair follicle drug delivery pathway. The schematic illustrates (1) nanoparticle entry into the hair follicle reservoir and (2) subsequent penetration through the HF barrier into the neighbouring tissue. The movement of hair can act as a 'geared pump' as the (a) cuticle cells that have a thickness ranging from 400 to 700 nm can allow particulate substances of similar dimensions to be transported into the HF; (b) The HF infundibulum, particularly the lower region, is notable due to the smaller and more fragmented corneocytes present, indicating an incomplete barrier that may allow the penetration of smaller substances; (c) Significant target areas within the hair follicle include the sebaceous gland, the bulge region containing stem cells, and the hair matrix cells. (Created in BioRender. Totea, A (2025) https://BioRender.com/r69e6gc).

psychological distress [5,8]. Additionally, chemotherapy can induce alterations in the hair's structure and texture, leading to changes that may persist even after treatment concludes. Some patients report that their hair grows back differently (curlier, coarser or thinner) compounding the emotional challenge posed by the initial hair loss, whilst (albeit less frequently) chemotherapy treatment can also cause permanent CIA (pCIA). While emotional distress caused by CIA is found in males as well, it predominantly affects females, as culturally hair loss is associated with a decline in vitality, strength, and overall health [9,10]. Thus, it is essential for healthcare providers to address these side effects, offering support and resources that can help patients navigate the complexities of their treatment journey while maintaining their quality of life [9,11].

Scalp cooling is the only known effective regulatory authorityapproved intervention for the reduction or prevention of CIA. Scalp cooling employs cooling (cold) caps supported by continuous-flow electronically controlled cooling devices that decrease the temperature of the scalp, ideally between 18 and 22 °C, before, during and postchemotherapy treatment. Typically, scalp cooling begins 20-30 min prior to the chemotherapy infusion and lasts for 20-150 min following infusion [5,6]. The efficacy of scalp cooling is supported by extensive clinical studies demonstrating its ability to significantly reduce hair loss, with a striking 50-65 % of patients developing only low-grade alopecia [12]. Although scalp cooling can be beneficial, its effectiveness varies among patients and tends to be diminished when used with certain highly genotoxic chemotherapy protocols. We propose that this variability in clinical outcomes may stem from inconsistent cooling of the scalp in some individuals. Clinical evidence supports this, indicating that the subcutaneous temperature of the scalp plays a crucial role in treatment success. Notably, scalp skin temperatures during cooling sessions can differ widely, ranging from approximately 10 °C-31 °C, and achieving a mean skin temperature around 18 °C has been linked to improved outcomes [5]. Our prior biological investigations into the cytoprotective effects of cooling, conducted using in vitro models,

suggest that the protective mechanism is not solely due to vasoconstriction, as previously thought [5]. Instead, additional mechanisms, including the direct reduction of cellular drug uptake, appear to contribute to the observed effects [6], highlighting the significance of temperature control in enhancing cooling efficacy against cytotoxicity [13].

We have recently provided, for the first time, evidence that cooling 'rescued' the matrix keratinocytes of human hair follicles (HFs) from chemotherapy-induced damage by attenuating the generation of reactive oxygen species (ROS) and subsequent oxidative stress, and that this cytoprotective effect was enhanced via co-application of antioxidants (AOs). Of note, optimal cooling (18 $^{\circ}$ C) alone effectively suppressed intracellular ROS and prevented chemotherapy-induced HF toxicity. By contract, sub-optimal (26 °C) cooling was less effective at protecting from such damage. Importantly, we showed that co-treatment with a panel of antioxidants (which included Resveratrol and N-acetylcysteine) potentiated the cytoprotective capacity of optimal and, most importantly, sub-optimal cooling. These findings supported a novel approach of combination of cooling with antioxidants for combating CIA [14]. Building upon the above evidence that co-application of an antioxidant dramatically enhances the ability of cooling (optimal and sub-optimal) to protect HFs from chemotherapy drug-induced damage [14], the present study has focused on developing a topical nanoparticle-based formulation aimed at targeted delivery of the antioxidant resveratrol (RV) to the follicular region of the skin, thus specifically exploring the potential of targeting RV to HFs as a precursor to scalp cooling to enhance its efficacy at preventing CIA.

RV, a natural polyphenol found in grapes, berries, and certain nuts, is recognised for its strong antioxidant properties and potential health benefits. Its ability to combat oxidative stress makes it a promising candidate for protecting human HFs from chemotherapy-induced damage [15,16]. Beyond its antioxidant effects, RV exhibits anti-inflammatory actions on the scalp, reducing irritation, itching, and discomfort associated with chemotherapy, thereby promoting a healthier environment for hair growth and minimising hair loss. Additionally, RV's capacity to stimulate collagen production enhances hair strength and elasticity, decreasing susceptibility to breakage and damage [17,18]. The selection of nanocarriers in our study as an antioxidant delivery system for RV is based on the skin's structure as the body's first line of defence, and on the physico-chemical properties of the AO. The skin is a highly protective barrier that allows molecules to penetrate via two pathways, along the skin appendages and into, or through the stratum corneum and the underlying tissues (Fig. 1). The skin's outermost layer, the stratum corneum, acts as a vital barrier that prevents the absorption of many substances, including drugs. This layer is mainly composed of corneocytes that are flat, non-nucleated, organelle-free epidermal cells embedded in an extracellular lipid matrix, as well as long chain ceramides, free fatty acids, triglycerides and cholesterol [9,19]. The lipid organisation in this layer differs from other biological membranes, as its hydration and impermeability are controlled by the intraand extracellular compartments, with about 80 % of the encompassing lipids being nonpolar. The remaining limited hydrophilicity is mostly due to the presence of hydrophilic groups inside the corneocytes, which can form hydrogen bonds [9,19-21].

Despite its highly protective role, stratum corneum has some potential routes for drug delivery, such as the HFs [22]. Vellus and terminal hair follicles can act as a shunt in increasing the absorption and penetration of substances applied onto the skin. By extending deep into the dermis, the hair follicles provide a target for potential drug absorption, also acting as a reservoir to maintain drug levels. In the lower infundibulum, the upper portion of the hair follicle, the corneocytes are smaller and 'crumbly', which renders them more penetrable. In this area the HF is also surrounded by a wide network of capillaries and a high density of antigen-presenting immune cells. When a drug penetrates the skin through the HFs, it firstly goes into the HF reservoir and further potentially through the barrier of the HF into the neighbouring tissue

 Table 1

 Components used in the formulation of 'blank' NLCs.

	Amount % w/v
Compritol® 888 ATO	2.04
SP Crodamol PC MBAL	0.36
Poloxamer® 188	1.2
Tween 80	0.6

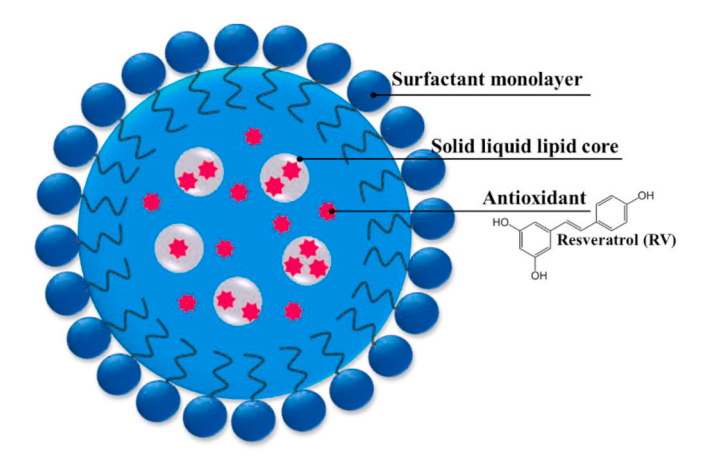


Fig. 2. Proposed structure of the formulated RV-loaded NLCs depicting the incorporation of RV in the solid lipid–liquid lipid core.

Table 2 Chromatographic conditions for the analysis of RV.

HPLC Parameter	Details						
Column	Gemeni 5 μ m C18 110 Å (Phenomenex, UK), 150 \times 2 mm i.d.						
Flow rate	0.5 ml/min						
UV detection	DAD detector; 305 nm for resveratrol						
Column temperature	25 °C						
Injection	10 μL						
Mobile phase	A = 1 % v/v acetic acid solution & B = methanol						
Method	Gradient						
Run time	20 min						
Elution condition	Time (min)	Mobile phase A (%)	Mobile phase B (%)				
	02:00	80	20				
	12:00	40	60				
	15:00	40	60				
	15:01	80	20				
	20:00	80	20				

[22]. However, the function of the HF as an important site for percutaneous absorption is often contentious, as besides the surface area created by HF openings in the skin, the secretion of sweat and sebum may delay the absorption of drugs and other xenobiotics [19].

Nanoparticles used for follicular delivery (Fig. 1) improve local bioavailability through enhanced transport into the HF and sebaceous glands as well as prolonged residence times. Efficient transport of materials into the HF depends on the interaction between the drug and the sebum, but even more importantly, on the choice of vehicle. Generally, the composition and physicochemical attributes of the nano-sized carriers, or their individual components, can either enhance or hinder their penetration and diffusion through the skin. Likewise, these attributes may also have an impact on whether they maintain their physical integrity when they interact with skin components.

Different types of nanoparticles may be employed for follicular drug delivery such as liposomes, polymeric nanoparticles and lipid nanoparticles [23,24]. Previous studies that focused on follicular drug delivery have also demonstrated that scalp massage induces hair shaft movement which pushes the particles deep into the follicles, which may increase the follicular penetration of nanoparticles [25]. The size of

nanoparticles plays a very important role, and it has been reported that small particles between 200 and 700 nm are able to penetrate through the skin and deposit around the follicular region [23,26]. Conversely, nanoparticles smaller than 100 nm may be transported into the systemic circulation [23,27–30].

The overall aim of this study was to formulate and characterise nanostructured lipid carriers (NLCs) to incorporate RV, thus providing an efficient targeted vehicle to deliver the AO to the follicular area of the skin. In addition to full characterisation of the NLC-based nanoformulations, the study also evaluated the extent and timing of the deposition of RV in the skin (including the HF regions) by assessment at 6-h and 24-h post-application of the RV-loaded NLC formulations.

2. Materials and methods

2.1. Materials

Resveratrol (RV) was acquired from Insight Biotechnology Limited (Wembley, UK). Tween 80 (Polysorbate 80), stearic acid, as well as HPLC-grade methanol and ethanol were sourced from Fisher Scientific UK Ltd (Loughborough, UK). Poloxamer® 188 (Pluronic F68) and eucalyptus oil (purity 100 %) were obtained from Merck Life Science UK Limited (Gillingham, UK). Compritol® 888 ATO (glyceryl behenate) was kindly provided by Gattefossée (Nanterre, France). SP Crodamol PC MBAL (propylene glycol dicaprylate/dicaprate) was generously supplied by Croda International Plc (Goole, UK), whilst oleic acid was a kind gift by H Foster (Goring-on-Thames, UK). Jojoba oil was purchased from Oleus (Holland & Barrett, UK).

2.2. Formulation of the nanostructured lipid carriers

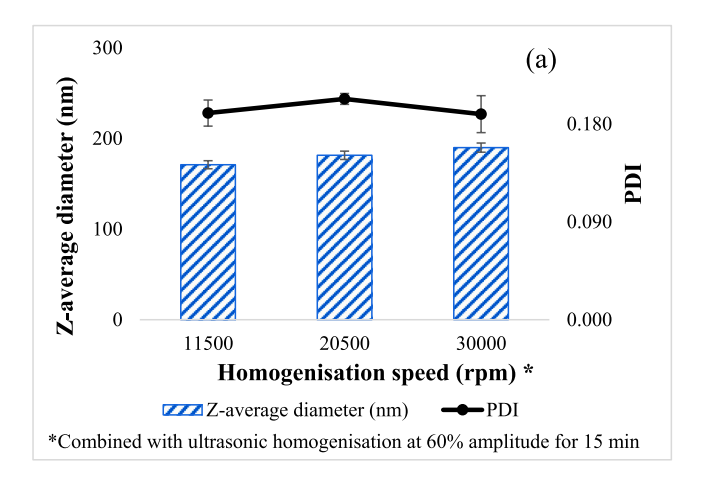
'Blank' NLCs (without the antioxidant) were prepared via high shear homogenisation combined with ultrasonic homogenisation, as outlined in Table 1. Initially the lipid phase containing Compritol® 888 ATO and SP Crodamol PC MBAL, and the aqueous phase prepared by mixing Poloxamer® 188, Tween 80 (TW80) and ultra-pure water, were heated separately to 85 °C and combined under high-shear conditions using UltraTurrax (T10). This was followed by pulsed ultrasonic homogenisation for 10 min at an amplitude of 60 % (20 s on/20 s off). Different homogenisation speeds ranging from 10,000 to 30,000 rpm, with or without ultrasonic homogenisation, were tested to determine the optimum process for the formulation of a stable 'blank' NLC dispersion. Furthermore, the effect of different liquid lipids on the size and polydispersity of the nanoparticle dispersions was also evaluated, with the incorporation of oleic acid, eucalyptus oil and jojoba oil in the formulation. The same procedure for the formulation of 'blank' NLCs was used to further prepare RV-loaded NLCs, with the incorporation of RV into the lipid phase, as shown in Fig. 2. Different concentrations of RV were explored, ranging between 10 and 50 mg, aimed at determining the physico-chemical properties and stability of the formulated dispersions.

2.3. Determination of the particle size, polydispersity index and zeta potential

Particle size (PS), polydispersity index (PDI) and zeta potential (ZP) were measured at 25 $^{\circ}\text{C}$ using dynamic light scattering (DLS) (Zetasizer Nano ZS; Malvern, Milan, Italy). PS and PDI were measured using backscatter detection at an angle of 173°, and sample preparation involved the dilution of the tested formulations with ultra-pure water (1:100 v/v). Following the same protocol for sample preparation, ZP was measured under an electrical field of 40 V/cm. All measurements were conducted in triplicate.

2.4. Stability studies

The stability of the 'blank' NLCs and RV-loaded NLCs was assessed



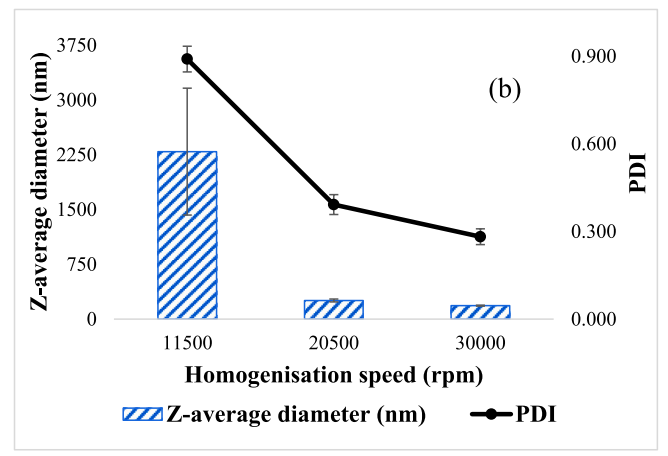


Fig. 3. The effect of high shear homogenisation speed on both Z-average diameter (nm) and PDI of 'blank' formulations prepared (a) in combination with ultrasonic homogenisation at an amplitude of 60 % (15 min) and (b) without ultrasonic homogenisation (bars represent mean \pm SD, n = 3).

over 3 months and 6 months respectively based on the changes in their PS, PDI and ZP upon their storage at 4 $^{\circ}$ C and/or 25 $^{\circ}$ C. At monthly intervals, samples were collected, diluted (1:100 w/v) and analysed using DLS.

2.5. High performance liquid chromatography

A Shimadzu HPLC system equipped with an auto sampler and a photodiode array detector was used for assay purposes. The analysis was carried out using a 15-cm long, 2-mm inner diameter stainless C18 Gemini column from Phenomenex, UK, and a mobile phase of methanol and acetic acid at gradient concentrations ranging from 20 % to 60 % methanol. The flow rate was set at 0.5 mL/min and the UV wavelength at 305 nm, the λ_{max} of RV. The chromatographic conditions for the analysis of RV are summarized in Table 2.

2.5.1. Method validation

The developed reversed phase HPLC method was validated as per ICH Guideline Q2(R1) by parameters: linearity range, precision, limit of quantitation (LOQ) and limit of detection (LOD). A good linearity was successfully achieved in the concentration range of 1 $\mu g/ml$ to $50~\mu g/ml$. The regression equation and correlation coefficient were found to y=155513x-59632 and $R^2=0.9998$. LOD and LOQ were determined as 0.7 ng/ml and 1.8 ng/ml respectively using regression analysis from the calibration curve. The intra and inter day precision was determined from an assay of freshly prepared 1, 5 and 15 $\mu g/ml$ standard RV solutions, repeatedly run on the same day or on three different days. Results were evaluated statistically in terms of standard deviation (RSD %) and were lower than 2 % RSD which complies with the acceptable criteria for

quality control of pharmaceutical preparations [31].

2.5.2. Entrapment efficiency

To determine the entrapment efficiency (EE%), each RV-loaded NLC dispersion was initially centrifuged using an Amicon® Ultra Centrifugal Filter (MWCO 10,000, Merk, Germany) at 4000 rpm on an Eppendorf Centrifuge. After 1 h, 1 ml of the filtered fraction was diluted with ethanol and further analysed for its RV content using HPLC to determine the quantity of free RV in the NLC dispersion. The total amount of antioxidant (free plus encapsulated RV) was obtained by diluting an aliquot of the dispersion in ethanol. The encapsulated amount of RV was determined by subtracting the free amount of RV from the total amount present in the dispersion. Finally, EE% was further calculated as shown in Equation (1).

$$EE\% = \frac{[Total \ amount \ of \ RV - Amount \ of \ free \ RV]}{Total \ amount \ of \ RV} x100 \qquad \text{(Equation 1)}$$

2.6. Digital microscopy

Morphological examination of the formulated NLCs was performed with a 4K VHX-7000 microscope from Keyence (Manchester, UK). A thin film of each RV-loaded NLC dispersion was allowed to dry out on a glass slide prior to being analysed.

2.7. Transmission electron microscopy

The surface morphology of the RV loaded and unloaded NLC dispersion was observed under transmission electron microscopy (TEM)

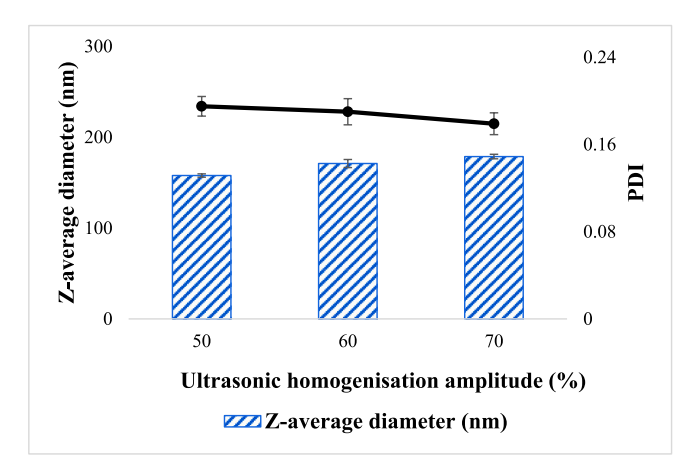


Fig. 4. The effect of ultrasonic homogenisation at different amplitudes (50 %, 60 % and 70 % for 15 min) on both Z-average diameter (nm) and PDI when combined with high shear homogenisation at 11500 rpm for 'blank' formulations prepared without the AO (bars represent mean \pm SD, n = 3).

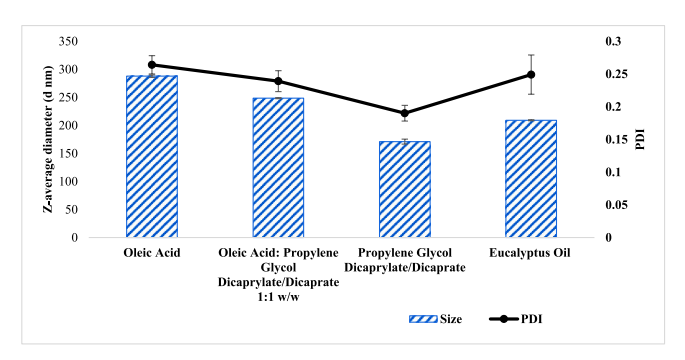


Fig. 5. The effect of liquid lipid variation on both Z-average diameter (nm) and PDI of 'blank' NLCs incorporating oleic acid, propylene glycol dicaprylate/dicaprate and eucalyptus oil (bars indicate mean \pm SD, n = 3).

(Hitachi SU8000). The observations were performed at an accelerating voltage of 30 kV and working distance of 8 mm, and sample preparation involved pipetting a drop of the 'blank' or RV-loaded NLC dispersion which was diluted 11 folds with deionised water onto a copper mesh. The excess sample was removed carefully using centrefeed roll. Uranyless non-radioactive lanthanide mixture was used as contrasting agent.

2.8. Ex-vivo permeation studies and differential skin stripping

Permeation studies were conducted to quantify the amount of AO localised in the skin. To mimic topical application of the formulation, the study was performed using vertical Franz diffusion cells (PermeGear, USA) with a receptor volume of 15 ml and an orifice area of 3.14 cm². Pig ears were obtained from a local slaughterhouse (Medcalf J & E Ltd, Huddersfield, UK) from a freshly slaughtered pig (used for food consumption). The ears were washed with deionised water and hairs were trimmed carefully with scissors. The pig ear skin was excised using a dermatome, as well as scalpel and forceps, and the subcutaneous tissue

was removed. The average thickness of the skin was \sim 0.5 mm. The skin was sliced and frozen (-20 °C) for future use. The receptor phase consisted of ethanol and PBS (pH 7.4) at a ratio of 1:1 v/v at 37 °C and sink conditions were taken into consideration. The skin was allowed to equilibrate for at least 1h in PBS (pH 7.4) before the experiment. The equilibrated skin was then mounted between the donor and receptor chambers and allowed to further equilibrate for 30 min. 1 ml of RVloaded NLC formulation was pipetted into the donor chamber. The donor chamber and the sampling port were further covered with parafilm during the test to minimise evaporation from the receptor chamber. The formulations tested were kept in contact with the tissue for 6-h or 24-h, whereupon excess formulation was gently removed, and the skin surface cleaned with dry paper. Further, stratum corneum was removed using a tape stripping method and the amount of AO present on the tapes was extracted in ethanol [32,33]. 15 tapes were used in total, depicting the deposition of the RV as formulation residual on the skin and in the stratum corneum, represented by Tape 1 and 2-15, respectively [32,34]. Subsequent to differential skin stripping, a drop of cyanoacrylate adhesive (Gorilla Super Glue®) was placed on the exposed skin areas. The adhesive was covered with a piece of tape (Scotch 3M Book Tape®), approx. 1.5 cm wide and 3 cm long under slight pressure. After 2 min, the cyanoacrylate polymerised, and the tape piece was removed with one quick movement. One more piece of tape was further used to strip the skin. The two collected adhesive tapes were used to determine the amount of AO around the hair follicles. The remaining skin was homogenised and added to a separate vial containing ethanol to extract the total amount to AO in the leftover skin [34]. HPLC was used to assess the amount of AO that permeated through the skin, as well as the AO content in different skin compartments with a focus on the follicular region. All the assays were conducted in triplicate

An unpaired *t*-test was performed to compare the levels of RV deposited in the follicular region between skin samples treated with the RV-loaded NLC formulation and a control sample.

3. Results and discussion

3.1. Formulation of the 'blank' nanostructured lipid carriers

Preliminary investigations concentrated on establishing 'blank' formulations-devoid of AO (RV)- prepared under various conditions. These studies were pivotal in achieving the optimal formulation parameters for follicular AO delivery, with the objective of enhancing percutaneous absorption and targeting HFs. It has been reported that the desired particle size is between 200 and 500 nm, as nanoparticles smaller than 100 nm could (potentially) enter systemic circulation [23, 26–30].

Preliminary formulation indicated that the optimal NLC dispersion parameters were achieved through high-shear homogenisation at 20,500 rpm, followed by ultrasonic homogenisation at 60 % amplitude (refer to Fig. 3 a). High-shear homogenisation alone showed limited efficiency in reducing particle size uniformly (Fig. 3 b), with the lowest particle size values being achieved upon mixing at 30,000 rpm (2293.0 \pm 868.5 nm), where foam formation and product loss was excessive, demonstrating thus the importance of optimising formulation parameters. The least amount of foam was formed upon high shear

Table 3 RV-loading, EE%, MPS, PDI and Zeta for RV-loaded NLC dispersions (n = 3).

Formulation code	RV Loading (mg/ml)	EE%		Z-average diameter (nm)		PDI		Zeta (mV)		Macroscopic Appearance
RV01	0.41	90.5	± 0.01	206.3	±3.5	0.22	± 0.011	-20.1	± 0.41	No sedimentation
RV02	0.68	45.8	± 0.13	320.3	± 3.3	0.25	± 0.011	-17.9	± 2.80	No sedimentation
RV03	1.13	28.9	± 0.06	448.2	± 0.4	0.24	± 0.066	-19.9	± 0.42	Sedimentation
RV04	1.48	12.6	± 0.40	492.3	± 6.3	0.38	± 0.013	-18.6	± 2.20	Sedimentation
RV05	1.89	1.5	± 0.47	799.2	± 10.0	0.53	± 0.040	-18.8	± 1.64	Sedimentation

homogenisation at 11,500 rpm and although particle size was large at 2293.0 \pm 868.5 nm and PDI 0.890 \pm 0.04 using this process alone, the addition of ultrasonic homogenisation (amplitude 60 % for 15 min) as a follow-up step, led to the formation of nanoparticles with a size of 171.0 \pm 4.4 nm and PDI of 0.190 \pm 0.01. PDI values smaller than 0.1 usually indicate monodisperse samples, while values over or equal to 0.4 suggest highly polydisperse samples, thus aiming for a PDI no higher than 0.2 ensures that the particles within the sample have a range of sizes, but the distribution is relatively narrow [35]. Adjusting the amplitude from 60 % to either 50 % or 70 % for ultrasonic homogenisation resulted in a particle size variation of less than 10 %, producing nanoparticles with sizes of 157.8 \pm 1.835 nm and 178.7 \pm 1.835 nm, respectively. The increase in amplitude during ultrasonic homogenisation not only caused the sample to overheat beyond 85 °C but also led to a gradual increase in particle size of over 10 %, with an 8 % decrease in the PDI values (Fig. 4). This phenomenon can be explained by transient cavitation effects induced by ultrasound. While transient cavitation is known to influence particle mobility and can contribute to particle size reduction through the breakdown of aggregates, the exact mechanisms responsible for nanoparticle formation remain under investigation. Elevated temperatures and changes in surface tension resulting from overheating may facilitate particle rearrangement and promote self-assembly, which can help prevent further aggregation [36].

The mean particle size and PDI were also greatly affected by the type of liquid lipid used (see Fig. 5). NLCs are formulated using a combination of solid and liquid lipids, resulting in an imperfect crystalline structure due to the inclusion of the liquid lipids. This structural imperfection facilitates high active compound loading within the lipid matrix, for which, the wide variety of lipid chemistries and structures enables the creation of NLCs with diverse properties and the ability to carry different actives. Nevertheless, multiple studies have demonstrated that the stability of NLCs is significantly influenced by the type and quantity of liquid oil incorporated into the lipid matrix [37-39]. Yang et al., 2014 [39] found that increasing the liquid lipid content improves dispersion stability by reducing the crystallisation and melting points of the lipid matrix and accelerates polymorphic transformations. These changes in turn promote the formation of more spherical particles, which tend to maintain their shape over extended periods, thereby enhancing suspension stability. Thus, the choice of the liquid lipid is crucial for optimising the performance and stability of NLC formulations.

Here, particle size was shown to be larger when oleic acid and eucalyptus oil were incorporated in the formulation, when compared to propylene glycol dicaprylate. This may be explained by the relatively short, saturated chains of the propylene glycol dicaprylate (a diester of caprylic acid), possibly leading to certain packing and crystallisation behaviours. On the other hand, eucalyptus oil is a volatile, complex essential oil with multiple components which can influence lipid matrix flexibility. Oleic acid is an unsaturated fatty acid that tends to increase lipid fluidity and can lead to larger or more loosely packed particles. The increase in particle size aligned with larger PDI values, showing a 28 % increase in polydispersity for samples formulated with oleic acid and eucalyptus oil. Overall, the optimum formulation with the right balance of size and PDI was the one that incorporated propylene glycol dicaprylate only as the liquid lipid.

3.2. Formulation of RV loaded NLCs

The RV-loaded NLC dispersion, formulated as described in Section 2.2 with 10 mg RV (RV01, Table 3), exhibited a mean particle size diameter of 206.3 ± 3.50 nm, PDI 0.22 ± 0.01 and ZP -20.1 ± 0.41 mV. These results imply that the sample was moderately polydisperse and had good stability, with the particle size diameter potentially being suitable for follicular antioxidant delivery [23,26]. The gradual incorporation of RV in higher amounts into the NLC formulation (up to 2 % w/w) led to an increase in particle size, which reflects changes in the encapsulation capacity of the formulated nanoparticles. Apart from the

changes in the size, the stability of the dispersion started to decline as a result of unencapsulated RV [40], being suboptimal for RV concentrations in the sample above 1.13 mg/ml. The optimal stability, where no sedimentation was observed, was at RV concentrations in the sample below 0.68 mg/ml. In agreement with the size results, PDI was also shown to be affected by the increase in RV content, remaining under 0.4 for the samples having a RV concentration no higher than 1.13 mg/ml, showing thus moderate polydispersity. These results are in line with the entrapment efficiency (EE%) data collected via HPLC as described in Section 2.6. At a RV sample concentration of 0.41 mg/mL, EE% was at 90.5 \pm 0.01 %. However, as more AO was incorporated in the formulation, the EE% gradually started to decrease, which could potentially be due to the lipid matrix reaching its saturation point, causing undissolved RV to precipitate and form aggregates (clumps). This process can negatively affect how well the active is trapped inside the carrier and can also compromise the overall stability of the sample. In fact, for the final sample formulated with 50 mg RV (RV05), the process of determining EE% was challenging due to the excessive sample precipitation blocking the pores of the ultra-purification tubes even after dilution, forming a cake and potentially leading to inaccurate analysis [41]. This explains the resulting EE% of 1.5 \pm 0.47 %, which is not in agreement with the EE% for the other samples i.e. 90.5 ± 0.01 % for sample *RV01* which means approx. 9 mg of RV encapsulated, compared to approx. 7.9 mg RV encapsulated in sample RV05.

3.3. Stability studies

3.3.1. 'Blank' NLC dispersion

The 'blank' NLCs formulated without the AO were shown to have a particle size diameter of approximately 158.99 ± 8.11 nm following DLS testing (Fig. 6). The PDI was 0.17 ± 0.03 suggesting that the size distribution of the particles in the samples was moderately polydisperse. The formulated NLCs were shown to exhibit a negatively charged ZP value of -17.18 ± 2.65 mV suggesting that the dispersion may be relatively stable, with highly stable dispersions expected to have a ZP higher than ±30 mV [34]. The formulated 'blank' NLC dispersion was stable over a 3-month testing period at 4 °C (Fig. 6), with changes in the particle size diameter, PDI and zeta potential under 10 %.

Upon storage at 25 °C, the 'blank' NLC formulation showed moderate instability, as observed from the increase in size and PDI, to 220.1 \pm 46.2 nm and 0.25 \pm 0.04 respectively (Fig. 7). The 'blank' NLC dispersion formulated was of a translucent white colour, and no sedimentation was observed at the end of the 3-month testing period under the tested conditions (4 °C and 25 °C).

3.3.2. RV-loaded NLC dispersion

Overall, the stability assessment of the RV-loaded NLC formulation $\it RV01$ (loaded with 10 mg RV) over 6 months at 4 $^{\circ}\rm C$ offered key information about the robustness of the formulation and its potential storage behaviour. The particle size remained relatively consistent, with fluctuations under 10 % (Fig. 8). PDI also remained consistent during the testing period and was between 0.23 and 0.26, while ZP was also shown to remain stable around -20 mV. Overall, the RV-loaded NLC dispersion showed promising stability over the 6-months period of testing.

3.4. Microscopy

Digital microscopy provided valuable insights into the morphological characteristics of the RV-loaded NLCs (Fig. 9). Increasing the amount of RV incorporated into the NLC formulations beyond 1.13 mg/ml made the nanoparticles more readily visible under the microscope, likely due to enhanced contrast or particle size variations. In these same samples the distinct crystalline structures of unincorporated RV became apparent, indicating crystallisation outside the lipid matrix which may potentially impact the stability and efficacy of the NLC formulations. This agreed with the DLS and EE% results (Section 3.2) where increased

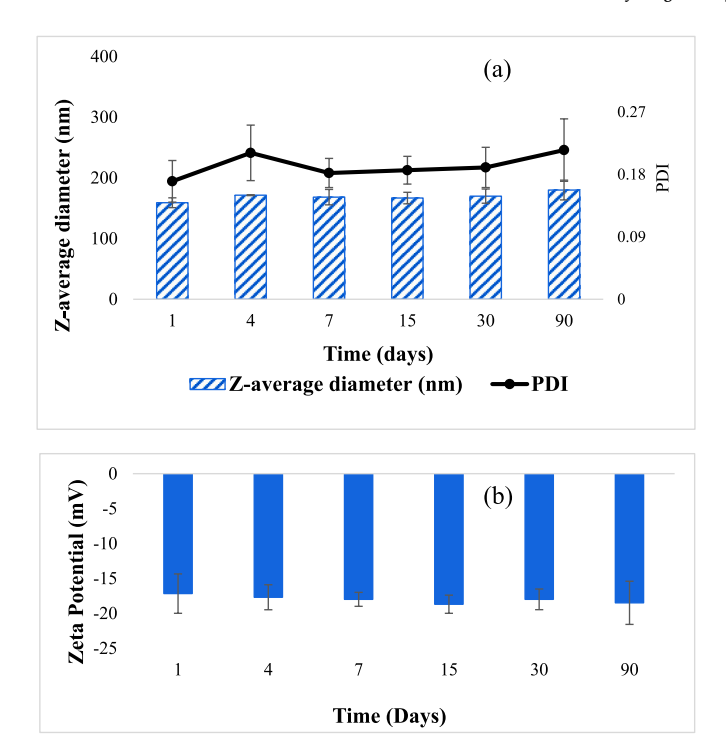


Fig. 6. 3-month stability assessment for 'blank' NLC formulation stored at 4 °C (dark conditions) showing changes in (a) Z-average diameter (nm) and PDI, and (b) zeta Potential (mV) (bars represent mean \pm SD, n=3).

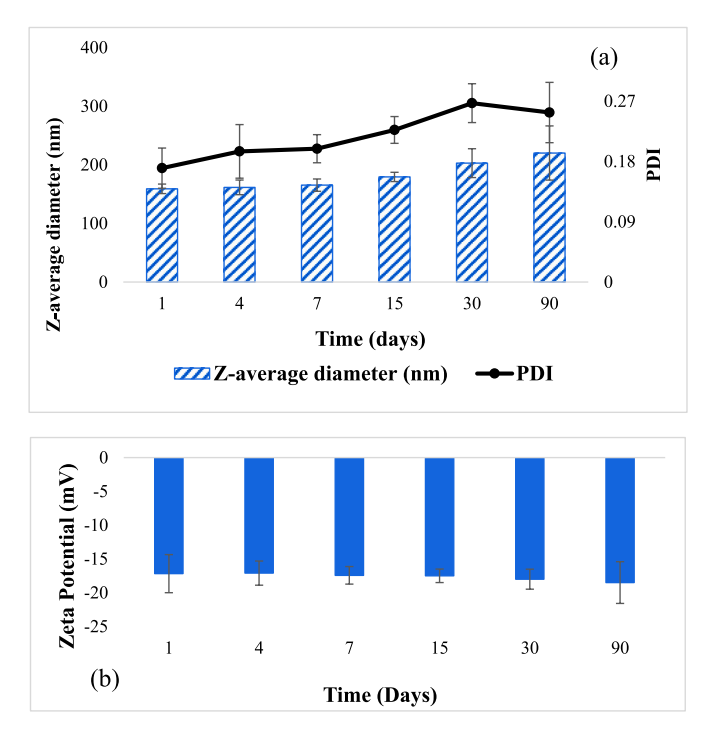


Fig. 7. 3-month stability testing for 'blank' NLC formulation stored at 25 °C (dark conditions) showing changes in (a) Z-average diameter (nm) and PDI, and (b) Zeta Potential (mV) (bars show mean \pm SD, n = 3).

aggregation was observed in the samples loaded with higher RV amounts.

TEM analysis of the 'blank' and RV-loaded NLCs revealed notable differences in their morphology related to the incorporation of RV (Fig. 10). In the RV-loaded NLC sample RV01, a distinct structural feature was observed: a white, crystalline core embedded within the lipid matrix. This core appeared as a densely packed, electron-dense

region, indicative of crystallised RV. Such a feature was absent in the 'blank' NLCs, confirming that RV was successfully encapsulated and crystallised within the lipid NLCs.

These findings suggest that the formulated RV-loaded NLCs possess a Type I structure, characterised by imperfect crystals (Fig. 11). The presence of these imperfect crystals indicates a disordered crystal lattice, which can enhance AO entrapment by allowing RV to exist within the

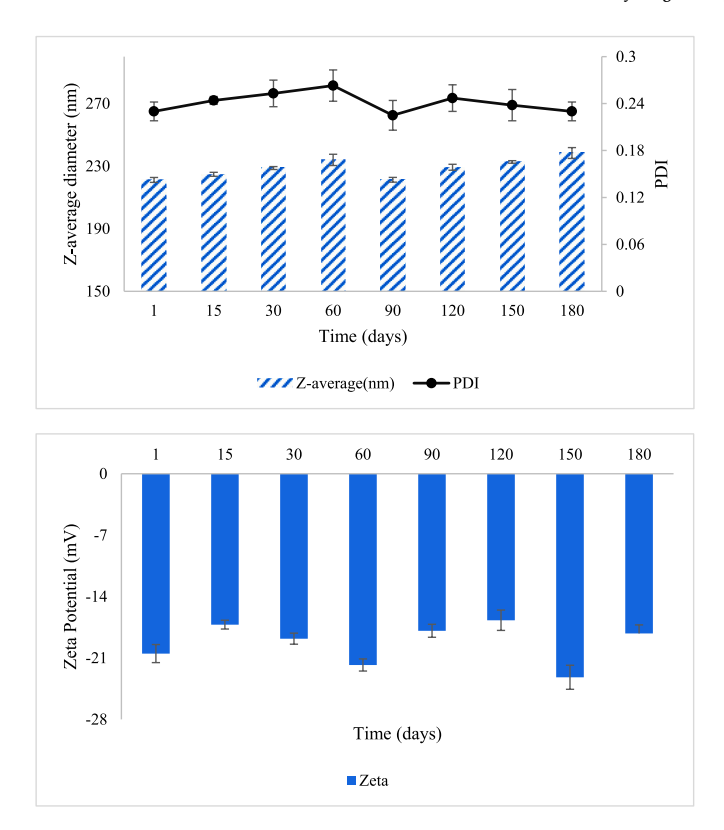


Fig. 8. 6-month stability assessment for the RV-loaded NLC formulation *RV01* stored at 4 $^{\circ}$ C (dark conditions) showing changes in (a) Z-average diameter (nm) and PDI, and (b) Zeta Potential (mV) (bars indicate mean \pm SD, n = 3).

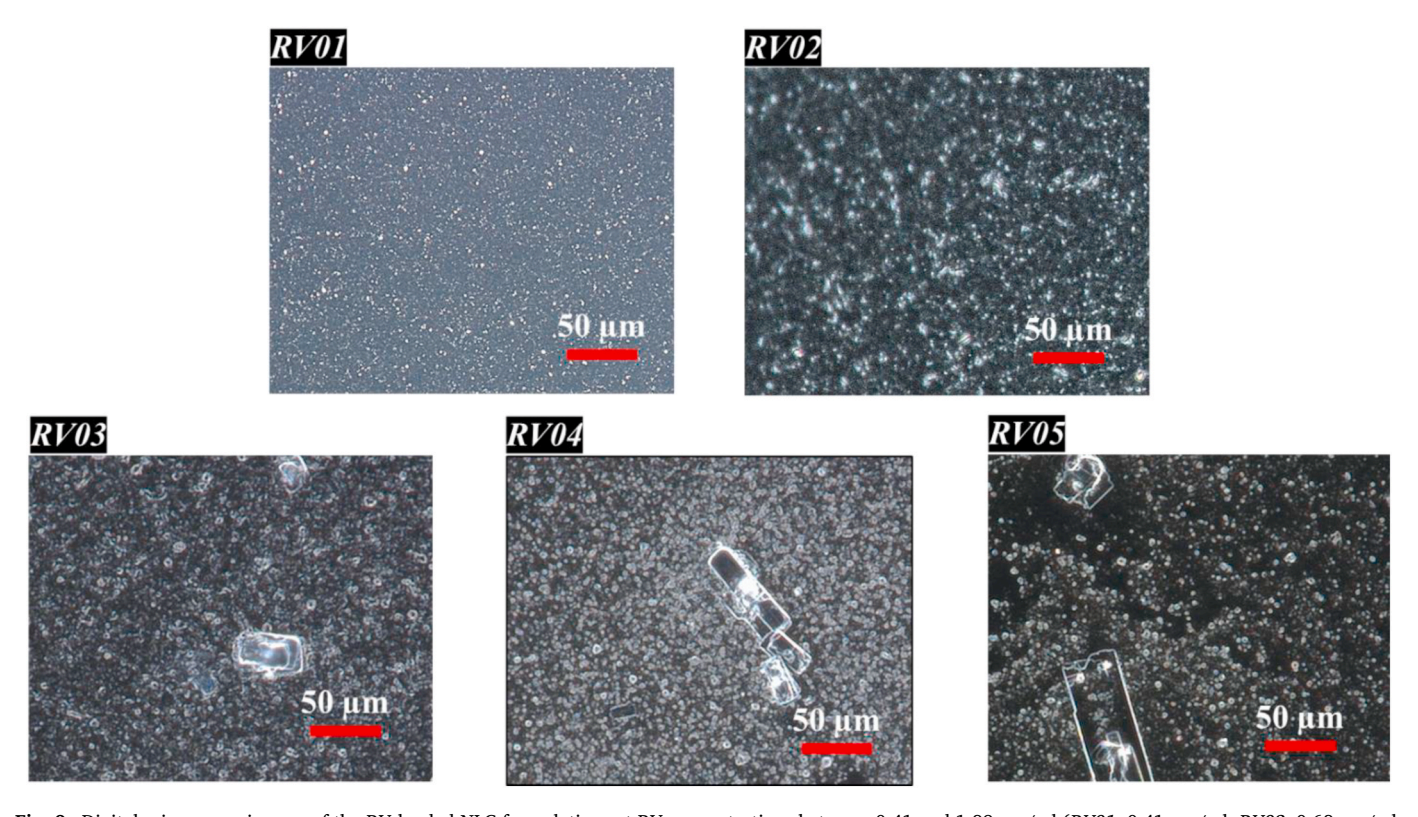
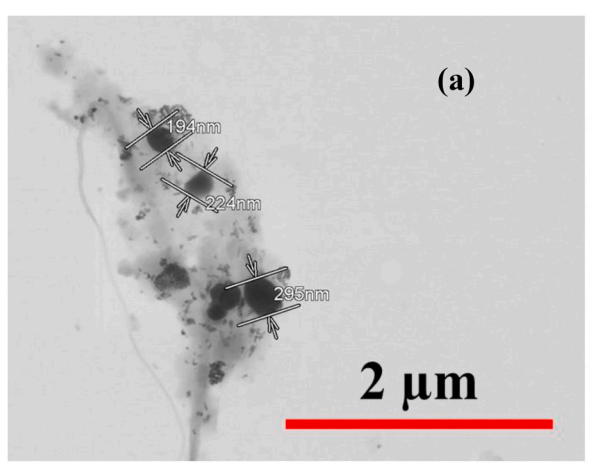


Fig. 9. Digital microscopy images of the RV-loaded NLC formulations at RV concentrations between 0.41 and 1.89 mg/ml (RV01: 0.41 mg/ml; RV02: 0.68 mg/ml; RV03: 1.13 mg/ml; RV04: 1.48 mg/ml; RV05: 1.89 mg/ml).



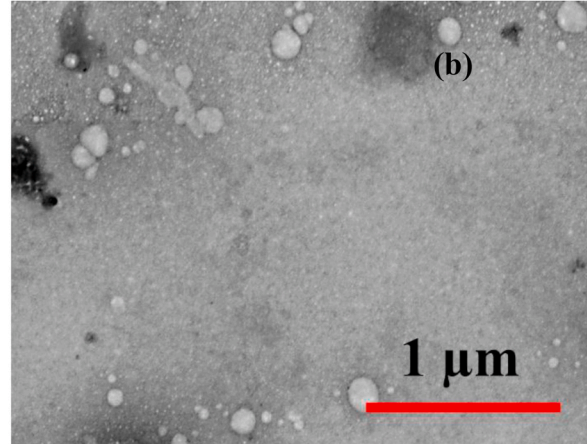


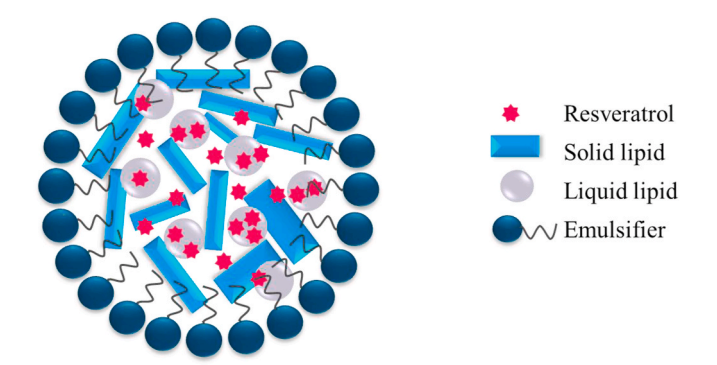
Fig. 10. TEM microscopy images showing the morphology of (a) 'blank' NLCs and (b) RV-loaded NLC sample RV01.

matrix as disordered crystals in molecular form or amorphous clusters. The inclusion of the liquid lipid (propylene glycol dicaprylate/dicaprate) in the formulation contributes to this irregularity of the solid matrix, increasing the capacity for AO incorporation. Previous studies by Müller et al. (2002) [42] and Mall et al. (2024) [43] showed that this structural arrangement may also improve the stability and controlled release profile of the RV-loaded NLCs.

3.5. Permeation studies

Studies involving differential skin stripping and cyanoacrylate skin surface biopsy conducted at 6- and 24-h following application on pig skin of the RV-loaded NLC formulation (RVI, loaded with 10 mg RV) demonstrated that RV can penetrate to the follicular region of the skin within 6 h in quantities significantly higher (p < 0.05) than a control sample (Fig. 13). The control sample was prepared by incorporating RV at the equivalent amount present in the RV-loaded NLC dispersion (10 mg) in a w/o emulsion prepared using jojoba oil (7.5 % w/w), SP Crodamol PC MBAL (propylene glycol dicaprylate/dicaprate) 15 % w/w, stearic acid (0.6 % w/w), and Tween 80 (8.5 % w/w).

Fig. 12 depicts the deposition of the RV as formulation residual on the skin and in the stratum corneum, in addition to the cyanoacrylate biopsy representing the deposited RV in the HF reservoir. The results showed the presence of higher amounts of the AO in the stratum corneum and follicular region at 6-h, when compared to the skin analysed at 24-h. This pattern is corroborated by the data shown in Fig. 13, which depicts the amount of RV in the residual skin, where similar levels of the active compound were observed at both time points, $10.02 \pm 4.14 \, \mu g/ml$ at 6-h, and $10.85 \pm 3.24 \, \mu g/ml$ at 24-h. These findings suggest that



 ${\bf Fig.~11.~Schematic~illustration~of~proposed~organisation~of~the~RV-loaded~NLCs~demonstrating~an~imperfect~Type~I~structure.}$

RV penetration is most prominent at 6 h, with levels decreasing or stabilising by 24-h. However, it is important to consider that these results may have been affected by the variability in skin absorption dynamics or other experimental factors.

The cumulative RV permeation was found to be 46.30 \pm 18.84 µg/cm² over 24-h, with a flux of 1.929 \pm 0.785 µg/cm²/h. The RV flux (J) was calculated from the quantity of RV, which permeated through the pig skin membrane, divided by the membrane surface and the time duration [µg/cm²/h] [44]. As reported in the literature, RV permeation through skin is low, with Hung et al. (2008) [45] reporting a RV flux from a saturated solution in pH 6 buffer through female nude mouse skin of 1.59 \pm 0.08 nmol/cm²/h (0.36 \pm 0.02 ng/cm²/h).

Skin permeation experiments after 24-h were also carried out for samples $\it RV02$ (RV concentration 0.68 mg/ml) and $\it RV03$ (RV concentration 1.13 mg/ml). The highest RV concentration in the follicular region was 4.10 µg/cm² of skin, which was recovered from skin treated with sample $\it RV03$ (RV concentration 1.13 mg/ml). This sample demonstrated moderate stability, accompanied by a significant presence of free RV in the formulation (Sections 3.2 and 3.4). The amount of RV in the follicular region was significantly lower (p < 0.05) in the skin samples treated with the formulations containing a lower amount of RV, $\it RV01$ (RV concentration 0.41 mg/ml), $\it RV02$ (RV concentration 0.68 mg/ml), at 1.54 µg/cm² and 0.62 µg/cm² respectively, which may imply that to some degree the NLCs may facilitate the permeation into the skin of the unencapsulated particles due to their ability to interact with the skin's structure and properties, potentially disrupting the stratum corneum and facilitating deeper penetration.

Overall, the results highlighted the capabilities of the formulated NLCs to deliver RV to the follicular region of the skin which is highly important for the intended use of the formulation in the protection of HFs from chemotherapeutic agents (Fig. 14). The accumulation of RV in both the epidermis and dermis was similar at both 6-h and 24-h demonstrating the rapid permeation of the particles into the skin and the release of RV in the skin appendages, such as HFs and glands as primary sites for nanoparticle deposition, allowing entry until nanoparticle degradation occurs. The enhanced penetration of NLCs is likely attributed to their smaller particle size and lower surface charge, which facilitate deeper tissue infiltration.

It is reasonable to assume that lipid nanoparticles can interact with cutaneous lipids in the skin and even potentially melt, leaving behind a lipid film with moisturising effects. At the same time, these nanoparticles can also penetrate the skin and its appendages, and it should be noted that hydrated skin is more permeable than dry skin, thus enabling the release of active ingredients from these lipid nanoparticles and establishing a sustained-release depot [19].

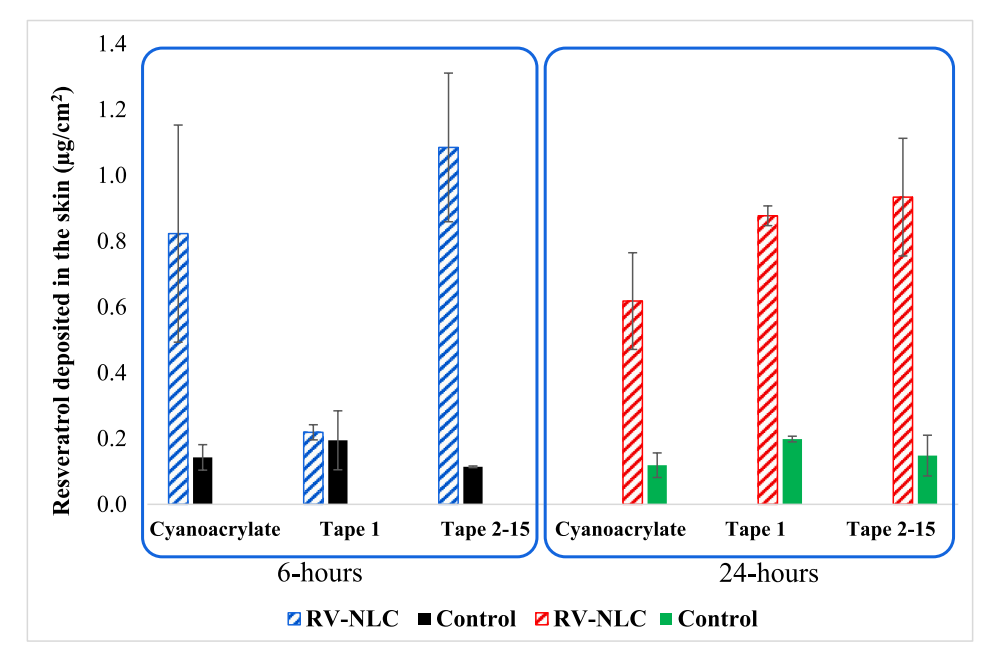


Fig. 12. Detection of amount of RV penetrating the skin using RV-NLC formulations loaded with 10 mg RV (RV01) and the control after 6-h and 24-h (mean \pm SD, n = 3).

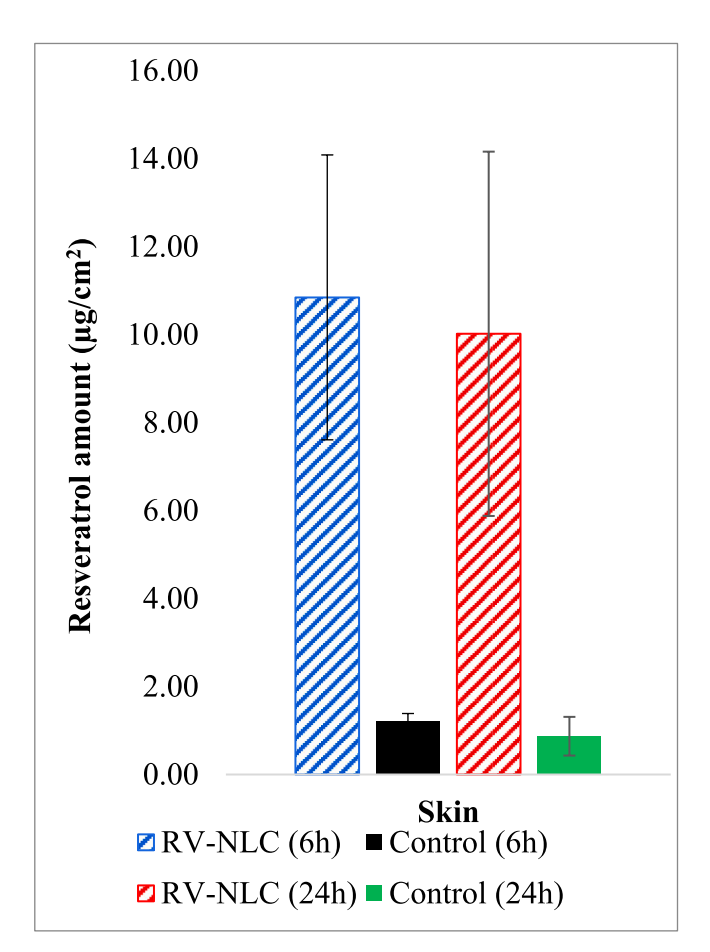


Fig. 13. Detection of amount of RV penetrating the deeper part of skin from RV01 formulation (loaded with 10 mg RV) and the control after 6-h and 24-h (mean \pm SD, n = 3).

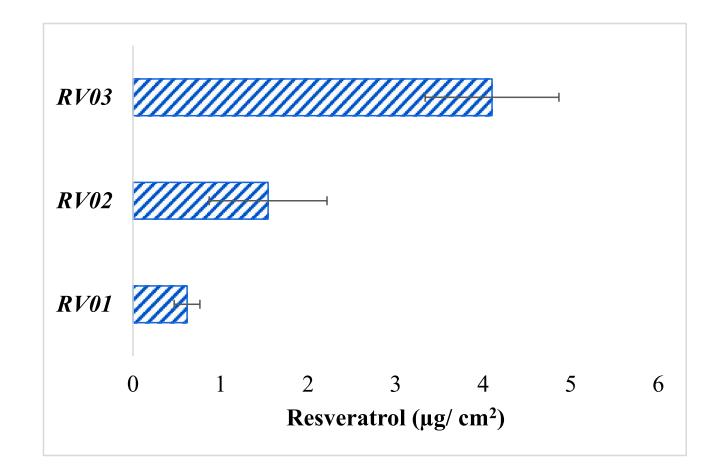


Fig. 14. RV amount in hair follicles after the application on skin surface for 24-h of samples *RV01*, *RV02* and *RV03* with a RV content of 0.41 mg/ml, 0.68 mg/ml and 1.13 mg/ml, respectively (0.618 \pm 0.147 $\mu g/cm^2$ for Sample *RV01*, 1.544 \pm 0.673 $\mu g/cm^2$ for Sample *RV02* and 4.102 \pm 0.764 $\mu g/cm^2$ for Sample *RV03*).

4. Conclusions

Our successful development of RV-loaded NLCs presents a promising strategy to enhance scalp cooling efficacy in preventing CIA. By optimising particle size and formulation stability, these NLCs effectively target hair follicle reservoirs, offering a localised antioxidant delivery combined with scalp cooling approach to mitigate follicular damage and thus hair loss. This innovative combinatorial approach holds the potential to improve patient outcomes by enhancing the clinical efficacy of scalp cooling and preventing the psychological impact of CIA. Future studies will be essential to evaluate the effectiveness of RV-loaded NLCs topically applied in conjunction with scalp cooling protocols in cancer chemotherapy patients, paving the way for comprehensive and patient-

centric care for hair preservation therapies during treatment. This approach also offers the exciting opportunity of developing further formulation types to encapsulate different antioxidants, thus tailoring antioxidant-plus-cooling combinations to specific chemotherapy drug regimens to maximise HF protection, reduce or prevent CIA, and transform the quality-of-life for patients worldwide thus 'changing the face of cancer'.

CRediT authorship contribution statement

A.M. Totea: Writing – review & editing, Writing – original draft, Methodology, Investigation, Formal analysis, Data curation. A. Thomas: Writing – review & editing, Methodology, Investigation. N.T. Georgopoulos: Writing – review & editing, Supervision, Project administration, Investigation, Funding acquisition, Conceptualization. B.R. Conway: Writing – review & editing, Validation, Supervision, Project administration, Methodology, Investigation, Funding acquisition, Formal analysis, Conceptualization.

Funding

AMT was supported by funding from Paxman Coolers Ltd (htt ps://paxmanscalpcooling.com/) via a High-Impact Innovation Fund (HIIF) grant (reference number 111979) awarded to Paxman as part of the Connecting Innovation programme, which was managed and delivered by the Leeds City Region Enterprise Partnership (LEP), with the West Yorkshire Combined Authority (WYCA) being its accountable body. No other authors were directly financially supported by Paxman. The authors declare that the sponsor was not involved in the design of the study; in the collection, analysis, and interpretation of data; in the writing of the manuscript; nor was the sponsor involved in the decision to submit the manuscript for publication.

Declaration of competing interest

NTG is a member of the scientific advisory board of Paxman, but he receives no consultancy-related income. NTG is co-inventor with Paxman Ltd in the patent no. WO2017220998A1 ('A composition for use in cooling therapy and treatment of chemically induced alopecia (CIA), said composition containing a reactive oxygen species (ROS) inhibitor' – published 2017). This does not alter the author's adherence to journal policies on sharing data and materials. The remaining authors declare no conflict of interest.

Data availability

Data will be made available on request.

References

- [1] W. Cao, K. Qin, F. Li, W. Chen, Comparative study of cancer profiles between 2020 and 2022 using global cancer statistics (GLOBOCAN), J. Nat. Cancer Center 4 (2) (2024) 128–134
- World Health Organization, Global cancer burden growing, amidst mounting need for services. https://www.who.int/news/item/01-02-2024-global-cancer-burdengrowing-amidst-mounting-need-for-services, 2024.
- [3] E. Bodó, D.J. Tobin, Y. Kamenisch, T. Bíró, M. Berneburg, W. Funk, R. Paus, Dissecting the impact of chemotherapy on the human hair follicle: a pragmatic in vitro assay for studying the pathogenesis and potential management of hair follicle dystrophy, Am. J. Pathol. 171 (4) (2007) 1153–1167.
- [4] M.B. Murphrey, J.H. Miao, P.M. Zito, Histology, Stratum Corneum, 2018.
- [5] C.J. Dunnill, W. Al-Tameemi, A. Collett, I.S. Haslam, N.T. Georgopoulos, A clinical and biological guide for understanding chemotherapy-induced alopecia and its prevention, Oncologist 23 (1) (2018) 84–96.
- [6] C. Dunnill, K. Ibraheem, M. Peake, M. Ioannou, M. Palmer, A. Smith, N. T. Georgopoulos, Cooling-mediated protection from chemotherapy drug-induced cytotoxicity in human keratinocytes by inhibition of cellular drug uptake, PLoS One 15 (10) (2020) e0240454.
- [7] M. Peera, L. Rose, L. Kaufman, E. Zhang, M. Alkhaifi, B. Dulmage, Hair loss: alopecia fears and realities for survivors of breast cancer—a narrative review, Ann. Palliat. Med. 13 (5) (2024) 1235–1245.

- [8] E.K. Choi, I.R. Kim, O. Chang, D. Kang, S.J. Nam, J.E. Lee, J. Cho, Impact of chemotherapy-induced alopecia distress on body image, psychosocial well-being, and depression in breast cancer patients, Psychooncology 23 (10) (2014) 1103–1110.
- [9] C. Paterson, M. Kozlovskaia, M. Turner, K. Strickland, C. Roberts, R. Ogilvie, P. Craft, Identifying the supportive care needs of men and women affected by chemotherapy-induced alopecia? A systematic review, J. cancer survivorsh. 15 (2021) 14–28.
- [10] S. Rosman, Cancer and stigma: experience of patients with chemotherapy-induced alopecia, Patient Educ. Counsel. 52 (3) (2004) 333–339.
- [11] T.C. Wikramanayake, N.I. Haberland, A. Akhundlu, A. Laboy Nieves, M. Miteva, Prevention and treatment of chemotherapy-induced alopecia: what is available and what is coming? Curr. Oncol. 30 (4) (2023) 3609–3626.
- [12] M.E. Lacouture, V. Sibaud, P.A. Gerber, C. Van den Hurk, P. Fernández-Peñas, D. Santini, ESMO Guidelines Committee, Prevention and management of dermatological toxicities related to anticancer agents: ESMO Clinical practice guidelines, Ann. Oncol. 32 (2) (2021) 157–170.
- [13] W. Al-Tameemi, C. Dunnill, O. Hussain, M.M. Komen, C.J. van den Hurk, A. Collett, N.T. Georgopoulos, Use of in vitro human keratinocyte models to study the effect of cooling on chemotherapy drug-induced cytotoxicity, Toxicol. Vitro 28 (8) (2014) 1266–1276.
- [14] Ibraheem, K., Smith, A., Collett, A., & Georgopoulos, N. T. Prevention of chemotherapy drug-mediated human hair follicle damage: combined use of cooling with antioxidant suppresses oxidative stress and prevents matrix keratinocyte cytotoxicity. Front. Pharmacol., 16, 1558593.
- [15] Y. Zhang, C. Ni, Y. Huang, Y. Tang, K. Yang, X. Shi, W. Wu, Hair growth-promoting effect of resveratrol in mice, human hair follicles and dermal papilla cells, Clin. Cosmet. Invest. Dermatol. (2021) 1805–1814.
- [16] F. Du, J. Li, S. Zhang, X. Zeng, J. Nie, Z. Li, Oxidative stress in hair follicle development and hair growth: signalling pathways, intervening mechanisms and potential of natural antioxidants, J. Cell Mol. Med. 28 (12) (2024) e18486.
- [17] K. Leis, K. Pisanko, A. Jundziłł, E. Mazur, K. Męcińska-Jundziłł, H. Witmanowski, Resveratrol as a factor preventing skin aging and affecting its regeneration, Adv. Dermatol. Allergol.Postepy Dermatol. i Alergologii 39 (3) (2022) 439–445.
- [18] X. Zhang, J. Hao, T. Lu, Y. Dong, Y. Sun, Y. Yu, H. Hu, Resveratrol-Loaded versatile nanovesicle for alopecia therapy via comprehensive strategies, Int. J. Nanomed. (2024) 13875–13900.
- [19] E.B. Souto, J.F. Fangueiro, A.R. Fernandes, A. Cano, E. Sanchez-Lopez, M.L. Garcia, A.M. Silva, Physicochemical and biopharmaceutical aspects influencing skin permeation and role of SLN and NLC for skin drug delivery, Heliyon 8 (2) (2022) e08938.
- [20] J.A. Bouwstra, M. Ponec, The skin barrier in healthy and diseased state, Biochim. Biophys. Acta, Biomembr. 1758 (12) (2006) 2080–2095.
- [21] P.W. Wertz, Stratum corneum lipids and water, Exog. Dermatol. 3 (2) (2005) 53–56.
- [22] N.A. Monteiro-Riviere, Toxicology of the Skin, CRC Press, 2010.
- [23] Y. Gu, Q. Bian, Y. Zhou, Q. Huang, J. Gao, Hair follicle-targeting drug delivery strategies for the management of hair follicle-associated disorders, Asian J. Pharm. Sci. 17 (3) (2022) 333–352.
- [24] S. Tampucci, V. Paganini, S. Burgalassi, P. Chetoni, D. Monti, Nanostructured drug delivery systems for targeting 5-α-reductase inhibitors to the hair follicle, Pharmaceutics 14 (2) (2022) 286.
- [25] B. Müller, M. Van de Voorde (Eds.), Nanoscience and Nanotechnology for Human Health, John Wiley & Sons, 2017.
- [26] A. Verma, A. Jain, P. Hurkat, S.K. Jain, Transfollicular drug delivery: current perspectives, Res. Rep. Transdermal Drug Deliv. (2016) 1–17.
- [27] J.J. Otarola, A.K.C. Solis, M.E. Farias, M. Garrido, N.M. Correa, P.G. Molina, Piroxicam-loaded nanostructured lipid carriers gel: design and characterization by square wave voltammetry, Colloids Surf. A Physicochem. Eng. Asp. 606 (2020) 125396.
- [28] A. Beloqui, M.Á. Solinís, A. Rodríguez-Gascón, A.J. Almeida, V. Préat, Nanostructured lipid carriers: promising drug delivery systems for future clinics, Nanomed. Nanotechnol. Biol. Med. 12 (1) (2016) 143–161.
- [29] A. Garcês, M.H. Amaral, J.S. Lobo, A.C. Silva, Formulations based on solid lipid nanoparticles (SLN) and nanostructured lipid carriers (NLC) for cutaneous use: a review, Eur. J. Pharmaceut. Sci. 112 (2018) 159–167.
- [30] A. Patzelt, H. Richter, F. Knorr, U. Schäfer, C.M. Lehr, L. Dähne, J. Lademann, Selective follicular targeting by modification of the particle sizes, J. Contr. Release 150 (1) (2011) 45–48.
- [31] J. Ermer, H.J. Ploss, Validation in pharmaceutical analysis: part II: central importance of precision to establish acceptance criteria and for verifying and improving the quality of analytical data, J. Pharmaceut. Biomed. Anal. 37 (5) (2005) 859–870.
- [32] Bahjat Alhasso, et al., Development of a nanoemulgel for the topical application of mupirocin, Pharmaceutics 15 (10) (2023) 2387.
- [33] P.G. Kakadia, B.R. Conway, Design and development of essential oil based nanoemulsion for topical application of triclosan for effective skin antisepsis, Pharmaceut. Dev. Technol. 27 (5) (2022) 554–564.
- [34] A. Teichmann, S. Heuschkel, U. Jacobi, G. Presse, R.H. Neubert, W. Sterry, J. Lademann, Comparison of stratum corneum penetration and localization of a lipophilic model drug applied in an o/w microemulsion and an amphiphilic cream, Eur. J. Pharm. Biopharm. 67 (3) (2007) 699–706.
- [35] M.R.M.M. Danaei, M. Dehghankhold, S. Ataei, F. Hasanzadeh Davarani, R. Javanmard, A. Dokhani, Y.M. Mozafari, Impact of particle size and polydispersity index on the clinical applications of lipidic nanocarrier systems, Pharmaceutics 10 (2) (2018) 57.

- [36] K.L. López, A. Ravasio, J.V. González-Aramundiz, F.C. Zacconi, Solid lipid nanoparticles (SLN) and nanostructured lipid carriers (NLC) prepared by microwave and ultrasound-assisted synthesis: promising green strategies for the nanoworld, Pharmaceutics 15 (5) (2023) 1333.
- [37] C. Houacine, D. Adams, K.K. Singh, Impact of liquid lipid on development and stability of trimyristin nanostructured lipid carriers for oral delivery of resveratrol, J. Mol. Liq. 316 (2020) 113734.
- [38] F. Saporito, G. Sandri, M.C. Bonferoni, S. Rossi, C. Boselli, A. Icaro Cornaglia, F. Ferrari, Essential oil-loaded lipid nanoparticles for wound healing, Int. J. Nanomed. (2018) 175–186.
- [39] Y. Yang, A. Corona III, B. Schubert, R. Reeder, M.A. Henson, The effect of oil type on the aggregation stability of nanostructured lipid carriers, J. Colloid Interface Sci. 418 (2014) 261–272.
- [40] I. Waheed, A. Ali, H. Tabassum, N. Khatoon, W.F. Lai, X. Zhou, Lipid-based nanoparticles as drug delivery carriers for cancer therapy, Front. Oncol. 14 (2024) 1206001
- [41] Y. Chen, J. Nan, A strategy to alleviate membrane fouling by optimizing the structure of the cake layer formed by flocs deposited directly on the membrane in the ultrafiltration process through coagulation and nanoscale Fe3O4/Fe3O4@ SiO2 load, J. Membr. Sci. 680 (2023) 121729.
- [42] R.H. Müller, M. Radtke, S.A. Wissing, Solid lipid nanoparticles (SLN) and nanostructured lipid carriers (NLC) in cosmetic and dermatological preparations, Adv. Drug Deliv. Rev. 54 (2002) S131–S155.
- [43] J. Mall, N. Naseem, M.F. Haider, M.A. Rahman, S. Khan, S.N. Siddiqui, Nanostructured lipid carriers as a drug delivery system: a comprehensive review with therapeutic applications. Intelligent Pharmacy, 2024.
- [44] C. Bartos, P. Szabó-Révész, T. Horváth, P. Varga, R. Ambrus, Comparison of modern in vitro permeability methods with the aim of investigation nasal dosage forms, Pharmaceutics 13 (6) (2021) 846.
- [45] C.F. Hung, Y.K. Lin, Z.R. Huang, J.Y. Fang, Delivery of resveratrol, a red wine polyphenol, from solutions and hydrogels via the skin, Biol. Pharm. Bull. 31 (5) (2008) 955–962.